High Pressure Raman Spectroscopy of Single Crystals of Hexahydro-1,3,5-trinitro-1,3,5-triazine (RDX)

ARTICLE *in* THE JOURNAL OF PHYSICAL CHEMISTRY B · MAY 2007

Impact Factor: 3.3 · DOI: 10.1021/jp0681092 · Source: PubMed

High Pressure Raman Spectroscopy of Single Crystals of Hexahydro-1,3,5-trinitro-1,3,5-triazine (RDX)

Zbigniew A. Dreger* and Yogendra M. Gupta

Institute for Shock Physics and Department of Physics, Washington State University, Pullman, Washington 99164-2816

Received: November 27, 2006

To gain insight into the high-pressure polymorphism of RDX, an energetic crystal, Raman spectroscopy results were obtained for hydrostatic (up to 15 GPa) and non-hydrostatic (up to 22 GPa) compressions. Several distinct changes in the spectra were found at 4.0 ± 0.3 GPa, confirming the α−γ phase transition previously observed in polycrystalline samples. Detailed analyses of pressure-induced changes in the internal and external (lattice) modes revealed several features above 4 GPa: (i) splitting of both the A′ and A″ internal modes, (ii) a significant increase in the pressure dependence of the Raman shift for NO_2 modes, and (iii) no apparent change in the number of external modes. It is proposed that the α−γ phase transition leads to a rearrangement between the RDX molecules, which in turn significantly changes the intermolecular interaction experienced by the N−O bonds. Symmetry correlation analyses indicate that the γ-polymorph may assume one of the three orthorhombic structures: D_{2h}, C_{2v}, or D_2. On the basis of the available X-ray data, the D_{2h} factor group is favored over the other structures, and it is proposed that γ-phase RDX has a space group isomorphous with a point group D_{2h} with eight molecules occupying the C_1 symmetry sites, similar to the α-phase. It is believed that the factor group splitting can account for the observed increase in the number of modes in the γ-phase. Spatial mapping of Raman modes in a non-hydrostatically compressed crystal up to 22 GPa revealed a large difference in mode position indicating a pressure gradient across the crystal. No apparent irreversible changes in the Raman spectra were observed under non-hydrostatic compression.

I. Introduction

Understanding the response of energetic materials to high pressures is important for addressing issues related to sensitivity, performance, and safety. Because typical high explosives (HE) are organic molecular solids, they are highly compressible and can undergo polymorphic transformations. High-pressure polymorphism of HE may also influence shock sensitivity because different polymorphs of the same compound can have different sensitivity to shock wave initiation. Therefore, an understanding of HE polymorphisms is required for the proper characterization of the reactive behavior of explosive molecular solids.

Here, we report on the structural stability and high-pressure polymorphism of single crystals of hexahydro-1,3,5-trinitro-1,3,5-triazine (RDX, $(CH_2NNO_2)_3$). RDX, the cyclic trimer of methylenenitramine, is one of the most important crystalline energetic materials used extensively in explosives and monopropellants. The RDX molecule consists of three NO_2 groups bonded to the nitrogen atoms of a triazine ring (see Figure 1). In the solid state, RDX is known to exist in three polymorphs: α, β, and γ.[1−6]

The α-polymorph exists at ambient conditions and has an orthorhombic structure belonging to the *Pbca* space group with eight molecules per unit cell.[1,2] All molecules occupy sites of C_1 symmetry, but they possess C_s pseudosymmetry with two of the nitro groups in the axial (A) position with respect to the s-triazine ring and the third in an equatorial (E) position. This molecular conformation is usually referred to as the chair AAE conformer.

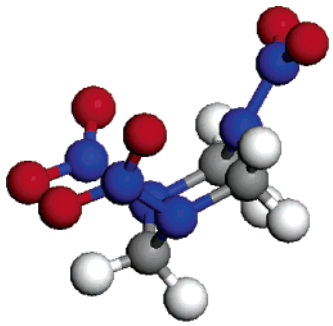

Figure 1. Equilibrium geometry of the RDX molecule in the α-polymorph. The molecule is projected on the (001) plane of the crystal. Legend: carbon, gray; nitrogen, blue; oxygen, red; hydrogen, white.

The β-polymorph is obtained either by evaporation of boiling solvent containing RDX,[1,4] deposition of RDX from solution on a glass substrate,[7] or under high temperature and high pressure.[6,8] The structure of this polymorph is unknown. However, on the basis of some similarities between the vibrational spectrum of the β-polymorph and that of RDX in the gas phase and in solution, the molecular symmetry for this polymorph was suggested to be C_{3v}.[5,9] Further experimental[10] and theoretical studies[11−12] for the gas phase showed that the C_{3v} conformer may assume a structure in which all of the NO_2 groups are in axial positions with respect to the s-triazine ring, forming the so-called AAA conformation.

The γ-polymorph was observed under high pressures above 3.8 GPa, using X-ray diffraction[3,14] and Raman[6] and IR spectroscopy.[8,15,16] X-ray diffraction results yielded a volume

* Corresponding author.

10.1021/jp0681092 CCC: $37.00
Published on Web 03/23/2007

change of ~1.6% at 4.0 GPa and suggested that the γ-polymorph, like the α-polymorph, may have an orthorhombic structure. Changes in vibrational spectra patterns above ~3.8 GPa were also indicative of the $\alpha-\gamma$ phase transition. Recently, on the basis of density functional theory (DFT) calculations and molecular dynamics (MD) simulations, it was suggested that the RDX molecule in the γ-polymorph can adopt the AEE conformation,[16] i.e., one nitro group in the axial position and two nitro groups in the equatorial position.

In summary, although the polymorphism of RDX has received considerable attention, previous studies provide rather scarce and sometimes contradicting information on the structural properties of non-ambient polymorphs. In particular, due to limited experimental data, the understanding of changes in RDX under high compression is incomplete. In this work, we provide more detailed information on the response of RDX to high pressure. We use high-pressure Raman spectroscopy as a sensitive tool for detecting changes in interactions and symmetries in the crystal by probing modifications in lattice dynamics, molecular arrangements, and conformations. To mitigate problems that are potentially encountered in studies under high pressure of molecular solids (random morphology of samples and uncertain compression conditions), the experiments reported here were performed with good quality single crystals and under well-controlled pressure conditions.

The purpose of our work was fourfold: (i) to examine changes in both internal and external vibrational modes to identify the factors that may destabilize the α-polymorph, (ii) to verify existing information regarding the $\alpha-\gamma$ phase transition, (iii) to further characterize the γ-polymorph, and (iv) to examine the effect of non-hydrostaticity on pressure-induced changes. It is also our intention to provide comprehensive experimental data for future theoretical studies.

The remainder of the paper is organized as follows. Experimental procedures including sample preparation, high-pressure generation, and Raman measurements are described briefly in the next section. Section III presents the experimental data and corresponding discussion regarding (i) pressure dependence of the internal and external vibrations, (ii) effect of non-hydrostaticity on vibrational spectra, and (iii) symmetry considerations inferred from the pressure-induced changes in the Raman spectra. The main findings of this work are summarized in Section IV.

II. Experimental Procedures

RDX single crystals were obtained from Dr. D. E. Hooks of Los Alamos. They were in the form of large slabs or small grains. The large crystals were suitably cleaved or cut into small pieces for high-pressure experiments. Single small grains were used without further processing. Typical dimensions of experimental single-crystal samples were ca. $0.1 \times 0.1 \times 0.03$ mm^3.

High pressures were generated in a modified Merrill−Bassett type diamond anvil cell (DAC). A stainless-steel gasket, preindented to 0.06 mm with a 0.18 mm hole drilled in the indentation, was used as a sample compartment. Cryogenically loaded argon or mineral oil was used as a pressure-transmitting medium. Those media were used to provide hydrostatic and nonhydrostatic compressions, respectively. Because of the presence of the strong Raman mode from the diamond anvils at 1333 cm^{-1}, experiments were also performed in a moissanite anvil cell (MAC), which provides a good optical window for Raman spectra in the range of 1200−1400 cm^{-1}.[17]

The ruby fluorescence method was used to monitor the pressure.[18] Pressure was determined from the frequency shift of the R-lines of the ruby crystal. By monitoring the separation and widths of both R_1 and R_2 lines, we confirmed that hydrostatic conditions were maintained up to 15 GPa in experiments with argon and to only 5.5 GPa with mineral oil.[19] For the non-hydrostatic case, the shift of the R_2 line was employed to determine the pressure in the cell.[20] The precision of our pressure measurements is estimated to be 0.05 GPa.

The 514.5 line from a cw Ar-ion laser (Innova 90-Coherent) was employed for Raman excitation. Two Raman spectrometers were used: (i) macroRaman based on a 0.6 m triple spectrometer (Spex 1877) provided spectral resolution of ~1.5 cm^{-1}; (ii) microRaman (T64000, JY-Horiba) equipped with a microscope (Olympus BX-40) provided spectral resolution of ~0.8 cm^{-1} and spatial resolution of 5 μm. The microRaman system was capable of measuring spectra to frequencies as low as 10 cm^{-1}. In both cases, less than 50 mW of power was incident on the sample. The crystals used in these studies had a random orientation with respect to the excitation beam.

All the experiments were carried out at room temperature and were repeated several times using different samples to check the consistency of the data. The Raman spectra were not corrected for the spectral sensitivity of the detection system. The experiments in the DAC were performed up to 15 GPa (hydrostatic) and 22 GPa (non-hydrostatic). The limit of 22 GPa in the non-hydrostatic experiment was determined by the thickness of the RDX crystal and the hole depth in the metal gasket. The maximum pressure reached in experiments with the MAC was 7 GPa. Pressure-induced shifts of overlapping bands were analyzed by fitting the Raman spectra to a Voigt (Gaussian−Lorentzian) function using a nonlinear least-squares algorithm. Experimental details regarding Raman and ruby fluorescence techniques can be seen elsewhere.[21]

III. Results and Discussion

A. Ambient Pressure. In the *Pbca* space group (D^{15}_{2h}) with C_s molecular symmetry, group theory predicts 57 internal and 45 external (lattice) vibrations for the RDX crystal at ambient conditions (α-polymorph): internal, $\Gamma_{int} = 31A' + 26A''$, and external, $\Gamma_{ext} = 6A_g + 6B_{1g} + 6B_{2g} + 6B_{3g} + 6A_u + 5B_{1u} + 5B_{2u} + 5B_{3u}$, modes.[22,23] All internal vibrations and external vibrations of even parity (g) are Raman-active. In Figure 2, we show the Raman spectra for the internal modes of an RDX single crystal at ambient pressure. Generally, the ambient pressure Raman spectra agree well with those obtained previously on powder samples[22] and from calculations on single molecules[11] (see Table 1). A detailed examination of the spectra reveals, however, a few extra peaks that were not reported before. Four of them are located around 2800 cm^{-1} (2750, 2776, 2842, and 2867 cm^{-1}). It seems that these peaks represent the vibrations of combinations or overtones of CH-scissors and/or CH-wagging modes rather than fundamentals vibrations. Because of their low intensity, they were not examined under high pressure and are not listed in Table 1. A different group of extra peaks is located between 1300 and 1600 cm^{-1} (1334, 1346, 1427, 1475, 1516, 1535, and 1600 cm^{-1}). These peaks are mostly the shoulders of well-defined peaks of fundamental vibrations. All these peaks can be plausibly associated with various binary combinations of fundamental vibrations.[24] Two peaks are also located at low frequencies, i.e., at 131 and 149 cm^{-1}. It is believed that these peaks represent fundamental modes and can be assigned to NO_2-torsional vibrations.[23,11]

B. Pressure Effects on Internal Vibrations. *1. Frequency Range 2800−3200 cm^{-1} (CH_2-Stretching Modes).* In Figures 3 and 4, we show pressure-induced changes in the CH-stretching

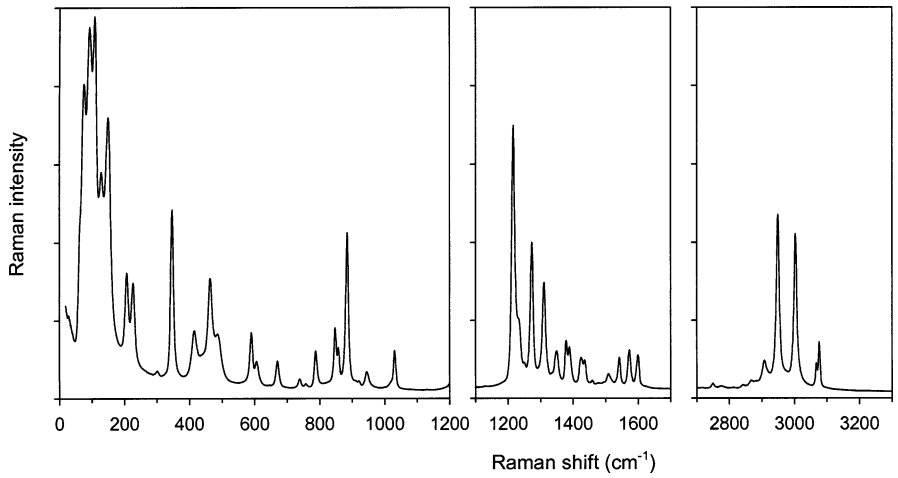

Figure 2. Raman spectra of RDX single crystal at atmospheric pressure. The laser beam was normal to the (210) plane of the crystal. For all frequency regions, the same scale is adopted to show the relative intensities and widths of different modes.

(symmetric and asymmetric) modes; Figure 3 presents typical spectra under several pressures, and Figure 4 presents the effect of pressure on Raman shifts of these modes. There are six modes predicted in this range; five of them are observed experimentally. With increasing pressure up to 4 GPa, all modes shift toward higher frequencies. The pressure dependencies of the Raman shifts ($d\nu/dp$, pressure coefficient) were obtained from the least-squares fits of the experimental data to either a linear or a polynomial equation. Table 1 includes the calculated coefficients together with the mode assignments and their frequencies. One can notice that the CH-stretching modes show on average larger pressure coefficients than other internal modes. Of particular interest in this pressure range is a significant increase in intensity of the two highest frequency peaks, 3067 and 3076 cm^{-1}. As can be seen in the inset in Figures 3 and 4, these two peaks have substantially different pressure dependence for the Raman shift. The increase of intensity occurs when the frequency of the ν_2 (3067 cm^{-1}) mode matches the frequency of the ν_1 (3076 cm^{-1}) mode. It may be that, due to some kind of a resonance, the total intensity of the combined peak is larger than the sum of intensities of separated peaks.

Several distinct features are observed above 4 GPa: (i) appearance of a new mode (ν^1), (ii) triple splitting of modes ν_3 and ν_4, (iii) changes in relative intensities among the modes, and (iv) discontinuities in the pressure dependence of Raman shifts. The occurrence of these features at this pressure is consistent with the previously reported[3,6,8,14] $\alpha-\gamma$ phase transition. The transition pressure was well reproducible to within $\pm(0.2-0.3)$ GPa in our experiments on single crystals. The distinctive change in the CH-stretching modes at 4 GPa, reflected in changes in the spectral envelope and the doubled number of modes, can be used as a signature of the $\alpha-\gamma$ phase transition in other types of loading.[25] Apart from a general increase in frequency under increased pressure, there were no other apparent changes in the spectra up to 15 GPa. We point out that, with decreasing pressure, the Raman spectra reverted to that of the α-phase. Also, the frequency shifts showed no pressure hysteresis within the error limits of the measurements.

2. Frequency Range 1200−1600 cm^{-1} (Contributions from NO_2-Stretching and CH_2-Scissor and -Wagging Modes). The pressure effect on Raman spectra in this frequency range is shown in Figure 5a, b. As already mentioned, this range includes several modes that can be classified as combination or overtones. All of these modes, except one at 1600 cm^{-1}, have a relatively low intensity. Several changes in the spectra can be noticed at the $\alpha-\gamma$ phase transition. They include, in order of appearance from high to low frequency (i) an increase in the number of modes, likely due to splitting, around 1600 cm^{-1}, 1550 cm^{-1} (NO_2-stretching), and ~1500 cm^{-1} (CH_2-scissors), (ii) merging of a triple peak at ~1430 cm^{-1} into one broad band, (iii) splitting of a doublet (ν_{18}, ν_{19}) into a triplet, and (iv) redistribution of intensity between the ν_{27} mode (N−C-stretching) and the ν_{26} mode (CH_2-twist). Some other details in pressure-induced changes in Raman modes can be noticed in Figure 6 and Table 1. We point out that the most characteristic feature of the transition is a significant increase in the pressure dependence of the Raman shifts of NO_2-stretching modes in the γ-phase compared to the α-phase. In this case, the pressure coefficient changes by almost a factor of 3 after the phase transition, indicating a much stronger sensitivity of these modes to compression in the γ-phase. Also, the overall number of modes increases in the high-pressure phase.

3. Frequency Range 100−1200 cm^{-1} (Contributions from N−N- and C−N-Stretching and Ring Modes). Figure 7a, b presents typical Raman spectra at several pressures in the frequency range 100−1200 cm^{-1}. Various changes in the spectra at 4 GPa confirm again the occurrence of the phase transition. Examination of the spectra shows clearly that several modes split. It is also noticeable that the splitting occurs mostly in the form of doublets. As can be seen, the splitting involves the following modes: N−C-stretch and CH_2-rock (ν_{28}, ν_{29}); N−N-stretch (ν_{30}); C−N-stretch (ν_{32}); N−NC(2)-umbrella and ring twist (ν_{46}, ν_{47}); molecular stretch (ν_{48}); N−NC(2)-umbrella (ν_{50}); and also ν'_{51}, ν_{53}. There is also one case where two modes, the ring bend and the N−NO_2-umbrella (ν_{36}, ν_{37}), split into a sequence of five peaks (see inset in Figure 7a). The original modes, ν_{36}, ν_{37}, and the new modes in the high-pressure phase exhibit some of the smallest pressure dependencies of Raman shifts among all of the RDX modes. The details of splitting are shown in Figure 8a, b and in Table 1. The extent of splitting varies among different modes from 7 cm^{-1} for ν_{36} to 21 cm^{-1} for ν_{29}. Above the phase transition, the rate of frequency shift decreases for almost every vibration in this frequency range.

As shown in Table 1, a typical value of $d\nu/dp$ in this frequency range varies between 3 and 8 $(cm\ GPa)^{-1}$. However, it is quite striking that all modes below 150 cm^{-1} (ν_{51}, ν'_{51}, ν_{52}, ν_{53}, and ν_{54}) exhibit two to three times larger pressure dependencies of Raman shifts than any other internal mode. Even though these modes were previously assigned to internal modes,[23] their behavior under pressure is more characteristic of external modes. This issue will be further discussed in the next section.

TABLE 1: Pressure Effect on Internal Raman Modes of RDX Crystal[a]

	1 atm					high pressure		
	frequency (cm^{-1})					phase I < 4 GPa	phase II	
mode	exptl, this work	exptl[b]	cald[c]	sym[b]	assign[c]	$d\nu/dp$[d] $(cm\ GPa)^{-1}$	> 4 GPa	freq
ν_1	3076	3075	3206	A′	CH st (eq)	2.3	4.4	3084
ν^1							16.3; 9.8	3147
ν_2	3067	3067	3199	A′	HCH st	7.1	10.2; 7.3	3096
ν^2							4.3	3096
ν^3							2.4	3067
ν_3	3003	3001	3081	A′	HCH st	8.6	7.5	3032
ν^4							5.4	3032
ν^5							4.6	3032
ν_4	2949	2949	3016	A′	CH st (ax)	10.2	7.6; 5.7	2994
ν^6							5.9	2973
ν^7							5.2; 3.6	2961
ν_5	2906		3015	A″	CH st (ax) or comb[e]	5.1		
ν^8							5.2	1613
ν_6	1600				comb/OT	1.7	5.1	1599
ν_7	1595	1593	1668	A′	O−N−O st (ax)	0.8	3.9	1590
ν_8	1573	1570	1648	A″	O−N−O st (ax)	1.7		
ν^9							3.8	1559
ν^{10}							2.8	1551
ν_9	1542	1538	1623	A″	O−N−O st (eq)	0.2	3.1	1542
ν_{10}	1535				comb/OT	1.7		
ν_{11}	1516				comb	3.6	3.3	1532
ν_{12}	1508	1508	1496	A′	CH_2 sci or comb[e]	2.0	2.0	1516
ν^{11}							2.0	1502
ν^{12}							0.6	1500
ν_{13}	1475				comb/OT	2.4	4.5	1471
ν_{14}	1460	1456	1480	A″	CH_2 sci	1.7	3.2	1459
ν^{13}							3.2	1452
ν_{15}	1436	1433	1468	A′	CH_2 sci	1.1	2.0	1433
ν_{16}	1427				comb	1.1		
ν_{17}	1422	1422	1420	A′	CH_2 wag or comb[e]	0.6		
ν_{18}	1388	1387	1406	A″	CH_2 wag	2.8	3.3	1402
ν^{14}							3.5	1392
ν_{19}	1377	1377	1374	A″	CH_2 tw	1.9	3.3	1376
ν_{20}	1346				comb	2.4	4.3	1355
ν_{21}	1351	1346	1362	A″	CH_2 wag or comb[e]	4.3	3.7	1362
ν_{22}	1334				comb	1.0		
ν_{23}	1309	1309	1362	A′	CH_2 tw, N−N st	4.9	6.0	1330
ν^{15}							5.0	1324
ν_{24}	1273	1273	1337	A′	CH_2 tw, N−N st (ax)	1.6		
ν'_{24}	1273		1299	A″	N−N st (ax), ONO st	4.1	6.5	1289
ν_{25}	1249		1296	A′	N−N st (ax)	5.1	4.0	1272
ν_{26}	1232	1232	1270	A″	CH_2 tw or comb[e]	3.7	3.7	1254
ν^{16}							3.2	1242
ν_{27}	1215	1214	1264	A′	N−C st	3.2	3.0	1231
ν_{28}	1031	1029	1153	A″	N−C st	8.5; 6.9	4.4	1055
ν^{17}							3.9	1072
ν_{29}	1023		1036	A″	CH_2 r	3.7	4.2	1023
ν^{18}							3.6	1045
ν_{30}	945	943	1011	A′	N−N st (eq)	6.0	3.7	966
ν^{19}							3.9	981
ν_{31}	920	920	951	A′	CH_2 r or comb[e]	3.8	2.8	934
ν_{32}	885	884	909	A″	C−N st	2.7	2.8	896
ν^{20}							2.8	889
ν_{33}	858	855	896	A′	C−N st	2.8	2.1	864
ν_{34}	848	847	870	A′	N−N st, NO_2 sci (ax)	4.3	3.7	854
ν_{35}	788	786	855	A′	C−N st, NO_2 sci	2.4	2.2	794
ν^{21}							1.4	768
ν_{36}	757	756	803	A′	ring b, NO_2 sci, or comb[e]	0.4	0.8	760
ν^{22}							0.8	753
ν_{37}	739	739	756	A′	N−NO_2 u (ax) or comb[e]	1.5	0.9	744
ν^{23}							0.9	736
ν_{38}	670	669	676	A′	ring b	5.1; 3.3	2.0	683
ν'_{38}						1.8	2.5	651
ν_{39}	607	605	651	A′	ring r	5.4	3.0	631
ν_{40}	590	589	610	A′	ring b	7.1; 6.4	3.1	617
ν_{41}	588		588	A′	ring tw	5.7; 4.8	2.5	607
ν_{42}	488	486	579	A′	ring tw, NO_2 sci	6.2	4.6	528
ν'_{43}						4.8	3.6	497
ν_{43}	464	463	463	A′	ring b (f), N−N st (eq)	5.8; 0.0	4.3	465

TABLE 1 (Continued)

	1 atm					high pressure		
	frequency (cm^{-1})					phase I < 4 GPa	phase II > 4 GPa	
mode	exptl, this work	exptl[b]	cald[c]	sym[b]	assign[c]	dν/dp[d] (cm GPa)$^{-1}$		freq
ν_{44}	429		438	A′	ring b (f)	3.3; 0.3	9.2; 1.0	450
ν_{45}	415	414	406	A′	ring b (flattening)	6.4; 3.4		
ν^{24}							1.5	409
ν_{46}	364		403	A″	N−NC(2) u (ax)	3.8	4.5	384
ν_{47}	347	347	371	A″	ring tw	4.9	3.8	364
ν^{25}							3.8	352
ν_{48}	301		325	A′	molecular st or OT[e]	7.1	3.3	327
ν^{26}							4.0	316
ν^{27}							4.8	265
ν_{49}	226	224	290	A″	ring rot	6.4	6.2	239
ν_{50}	207	205	229	A′	N−NC(2) u (eq)	6.7	5.6	232
ν^{28}							8.3; 6.7	215
ν'_{51}						20.7; 11.1	8.5; 1.5	210
ν_{51}	149				NO_2 tor?	18.7; 2.7	10.3; 3.0	190
ν_{52}	131				NO_2 tor?	21; 5.4	5.4	178
ν^{29}							8.7;3.1	167
ν_{53}	107	106	209	A″	molecular b	16.7; 8.7	10.5; 2.7	158
ν^{30}							7.6; 4.2	146
ν_{54}	90	90	107	A′	NO_2 tor (ax)	17.7; 3.3	7.6; 2.6	138

[a] Abbreviations: st, stretch; eq, equatorial; ax, axial; tw, twist; r, rock; b, bend; u, umbrella; rot, rotation; sci, scissor; f, fold; tor, torsion; comb/OT, combination or overtone. [b] Reference 22. [c] Reference 11. We chose to use the assignment from this reference despite that it differs in several instances with those given in refs 5 and 22. We believe that the assignment in ref 11 is more accurate because it was done with the assistance of visualization software. [d] The values of the pressure coefficients are obtained from the polynomial or linear equation. [e] Assignment from ref 24. The two values in the column correspond to the coefficients, respectively, at the beginning and the end of particular pressure range. Note that the modes existing at atmospheric pressure are denoted with subscripts and new modes with superscripts. Modes denoted with a prime emerge before the $\alpha-\gamma$ phase transition.

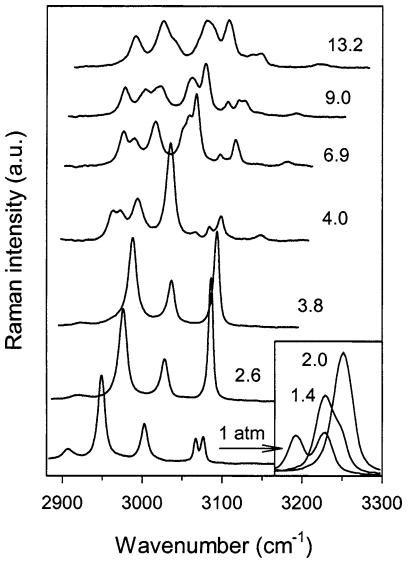

Figure 3. Raman spectra showing CH-stretching modes at several pressures. Pressure values (GPa) are shown next to each spectrum. The curves in this figure are vertically displaced for the sake of clarity. Inset presents details of evolution with pressure for modes located at 3076 and 3067 cm^{-1}.

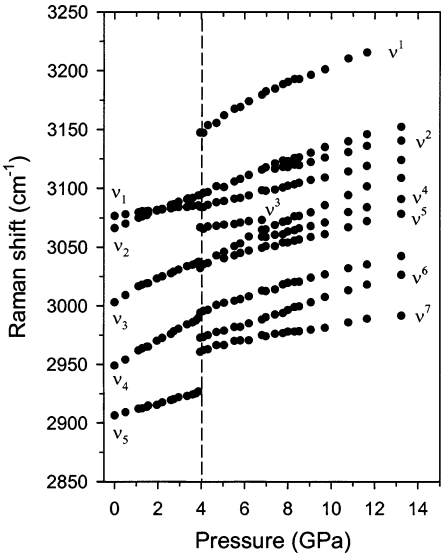

Figure 4. Pressure-induced shifts for CH-stretching modes. The vertical dashed line marks the onset of discontinuity. Note that the modes existing at atmospheric pressure are denoted with subscripts and new modes in high-pressure phase with superscripts.

It is also worth mentioning that in a few cases new features show up at pressures as low as ~2 GPa. An example involves the exchange of intensity between the ν_{42} and ν_{43} modes, and the emergence of a new mode, ν'_{43}, between them. Also, two other peaks of different frequencies, ν'_{38} and ν'_{51}, develop. One can notice that the occurrence of these features coincide with the crossing of Raman frequencies for ν_1 and ν_2 CH-stretching modes, mentioned above. It does not seem that these features indicate another phase transition. However, they may be meaningful precursors to the $\alpha-\gamma$ phase transition at 4.0 GPa.

C. Pressure Effect on External Vibrations. As stated above, group theory predicts 24 external (lattice) Raman active modes for RDX crystal. Twelve of these modes are librational and the other twelve are translational. The assignment of external modes in the RDX crystal was performed by Rey-Lafon et al.,[23] using polarized vibrational spectroscopy. Their results are presented in Table 2 and show that at ambient pressure all external modes are located below 80 cm^{-1}, occupying a very narrow frequency range of 60 cm^{-1}. As seen in Figures 9 and 10, we were able to distinguish 9 external modes from the low-frequency spectrum. Note that two higher frequency peaks at 90 and 107 cm^{-1} are assigned to internal modes according to predictions

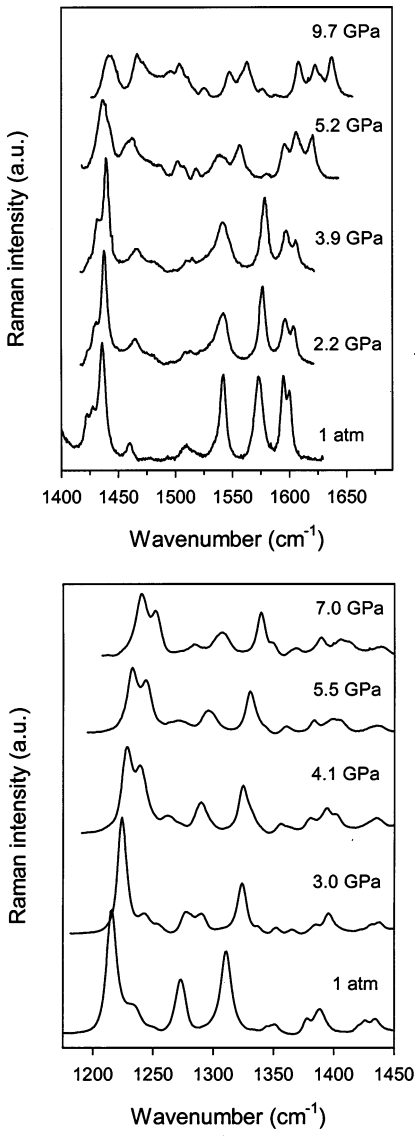

Figure 5. The effect of pressure on NO_2 and CH_2 vibrations. (a) Raman spectra in the frequency range 1400−1600 cm^{-1} at several pressures. (b) Raman spectra in the frequency range 1200−1400 cm^{-1}. Pressure values (GPa) are shown next to each spectrum. The curves in this figure are displaced vertically for the sake of clarity.

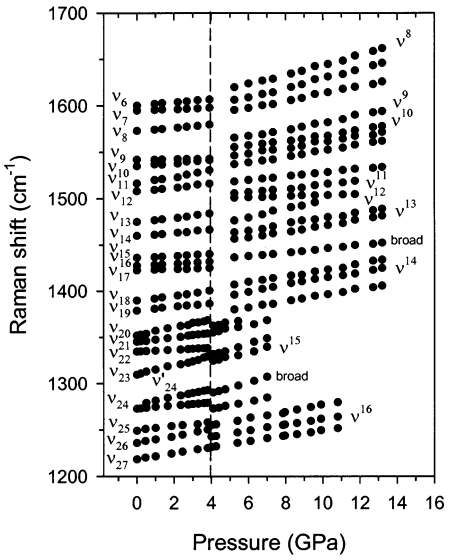

Figure 6. Pressure-induced shift of modes between 1200 and 1600 cm^{-1}. The vertical dashed line marks the onset of discontinuity. Note that the modes existing at atmospheric pressure are denoted with subscripts and new modes in high-pressure phase with superscripts.

from ref 23. The position of external modes with their tentative assignment at ambient pressure is given in Table 2. With increasing pressure, the spectrum evolves and some peaks that are not clearly seen at ambient conditions become better separated at higher pressures, e.g., L_{2-2}, L_{4-1}, L_{6-1}, L_{6-2}, L_{6-3}. It can be seen in Figure 10 and Table 2 that the external modes exhibit a large pressure dependence as can be expected for molecular solids.[26] The only exception is the lowest librational mode at 21 cm^{-1} (libration of the molecule about the *x*-axis), which hardly changes with pressure. On average, pressure-induced shifts of librational is less than the translational modes. The change in frequency of librational modes from 0 to 4 GPa is ∼40% compared to ∼60% for most of the translational modes. The pressure dependencies of Raman shifts are nonlinear for all the external modes; from 0 to 4 GPa, the dν/dp value decreases several times (see Table 2).

If the assignment of external modes in ref 23 is correct it would give a frequency separation between the internal and external vibrations as low as 14 cm^{-1}, at ambient pressure, and 8 cm^{-1} at 4 GPa. These values are relatively small compared to values in typical molecular solids,[26−30] which could indicate a small disparity between inter- and intramolecular bondings in the RDX crystal. Alternatively, the comparison of Figure 10 with Figure 8 reveals that low frequency internal modes, from ν_{51} to ν_{54}, have very similar pressure dependencies compared to the highest frequency external mode, L_{6-3}. Furthermore, the frequency separation between the highest frequency mode with large pressure dependence (ν_{51}) and the lowest frequency mode with small pressure dependence (ν_{50}) would be 58 cm^{-1}, at ambient pressure, and 30 cm^{-1} at 4 GPa. Therefore, it is possible that ν_{51} to ν_{54} modes are actually external modes, in contradiction to the previous assignment.[23] In such a case, the number of external modes observed at ambient pressure would be 13 instead of 9, from a total of 24. Because we have not performed the assignment of external modes, we use the assignment of ref 23 for the purpose of these studies. Very recently, this assignment was confirmed in ref 24. Thus, the RDX crystal represents an interesting case where low frequency internal modes act like external modes.

With the increase of pressure above 4 GPa, the spectral shape changes considerably as a result of the merging of some peaks into broad bands (see Figure 9). Nevertheless, we attempted to isolate peaks from the spectra. In Figure 11, we compare the result of spectral fitting of the γ-polymorph (6.1 GPa) with the fitting of spectra of the α-polymorph (4 GPa). As seen, the number of peaks in the γ-phase apparently increases slightly from 9 to 12. The extra couple of peaks that show up above the phase transition could be ones that were not well separated in the low-pressure phase. The pressure dependencies of the Raman shifts of external modes in γ-phase are noticeably smaller than at ambient conditions but to some extent higher than those just before the phase transition. This would indicate the hardening of the structure when pressure approaches the phase transition and some softening of the structure above the phase transition.

D. Effect of Non-hydrostaticity. Because of their low symmetry and low threshold for inelastic deformation, molecular crystals, including energetic crystals, are sensitive to non-hydrostatic compression. This often leads to irreversible changes in the crystal due to the formation of structural defects[31,32] and/or the initiation of chemistry.[33] In the present work, non-

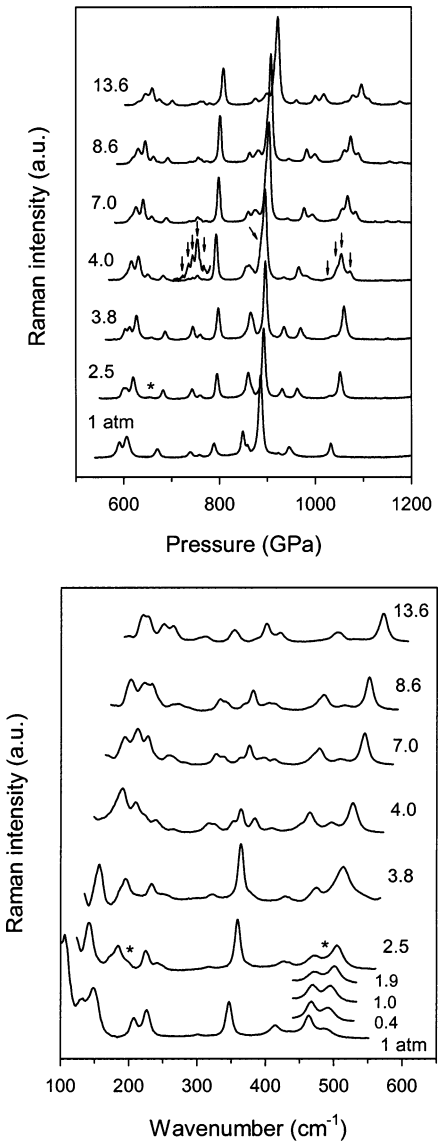

Figure 7. The effect of pressure on Raman modes in the frequency range 100−1200 cm^{-1}. The features labeled with an asterisk represent new peaks that emerged at ∼2.0 GPa. (a) Raman spectra in the frequency range 600−1200 cm^{-1} at several pressures. The arrows indicate splitting on some modes in the γ-polymorph. The feature at ∼750 cm^{-1} was magnified for the sake of clarity. (b) Raman spectra in the frequency range 100−600 cm^{-1} at several pressures. Note the exchange of intensity between peaks located at 464 and 488 cm^{-1} around 2.0 GPa. Pressure values are shown in GPa next to each spectrum.

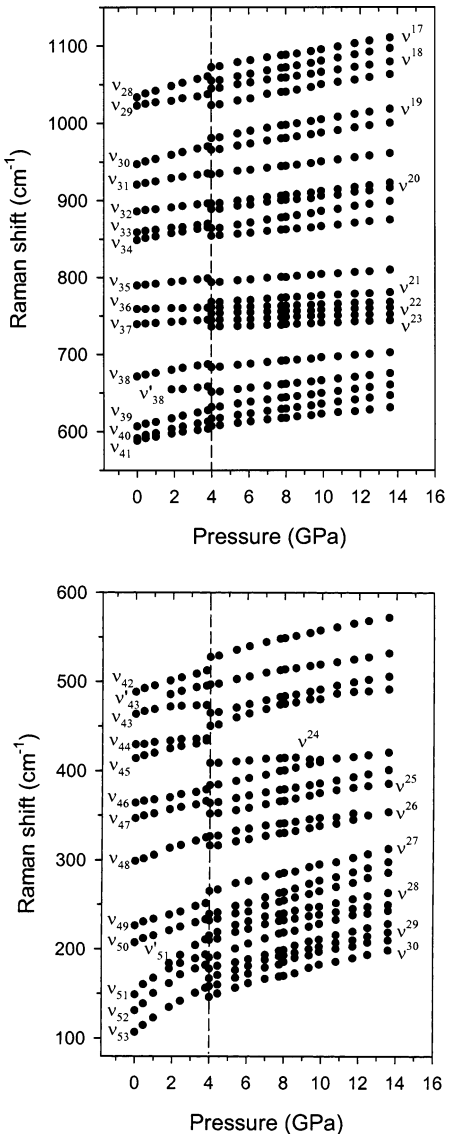

Figure 8. The effect of pressure on Raman shifts. (a) Frequency range 600−1200 cm^{-1}. (b) Frequency range 100−600 cm^{-1}. The vertical dashed line marks the onset of discontinuity. Note that the modes existing at atmospheric pressure are denoted with subscripts and new modes in high-pressure phase with superscripts.

hydrostatic compression was generated by using mineral oil as a pressure transmitting medium, which provides non-hydrostatic conditions above ∼5.5 GPa.[19] Because the pressure threshold for non-hydrostaticity in this medium was higher than 4 GPa, the $\alpha-\gamma$ phase transition was not affected: same changes in Raman spectra were observed with mineral oil as with hydrostatic argon.

Figure 12 presents an example of Raman spectra for the CH-stretching modes of the RDX crystal compressed hydrostatically and non-hydrostatically up to ∼13 GPa. It is clear that peaks in the spectrum under non-hydrostatic compression are broader than those under hydrostatic pressure. Due to an increased overlapping of peaks under non-hydrostatic conditions, the peak positions were not determined. However, a rough estimate indicates that the positions of the peaks differ compared to those under hydrostatic conditions.

More information on the behavior of the sample under non-hydrostatic compression was obtained by monitoring the spatial variation in one selected Raman mode across the crystal. For this purpose, we chose a high-intensity mode, ν_{32} (C−N-stretching) located at 885 cm^{-1} at ambient pressure. This mode maintains a high intensity in the γ-phase, and it can be separated effectively from other modes. For this measurement, we used the microRaman probe with a spatial resolution of ∼5 μm to map the spatial variation in the crystal. In Figure 13, we show the result of measurements under non-hydrostatic compression at ∼22 GPa. Many spots (100) regularly spaced over the area of 100 × 65 μm^2 of the crystal were mapped in this experiment. The spatial dependencies of the mode frequency and the mode width are presented in panels B and C. It is clear that the frequency of the mode changes significantly across the sample. If the edges of the sample are excluded from the estimate, the largest frequency difference between different spots is ∼13 cm^{-1}. Furthermore, if one assumes that the pressure dependence of the Raman shift in the γ-phase under non-hydrostatic compression is similar to that under hydrostatic compression, 2.8 $(cm\ GPa)^{-1}$, then, from differences in measured frequency

TABLE 2: Pressure Effect on External Raman Modes of RDX Crystal

	1 atm							high pressure		
	frequency (cm^{-1}) II									
	exptl, this	exptl[a]						phase I	phase	
mode	work	A_g	B_{1g}	B_{2g}	B_{3g}	calcd[a]	assign[a]	$d\nu/dp^b$ [cm GPa]$^{-1}$		freq
L_1	21	20	20	20	19	32	libr	2.8; 0.2	1.5; 0.8	38
L_{2-1}	29	33	28	29	37	46	libr	4.6; 2.6	5.7; 0.7	46
L_{2-2}	38							5.3; 2.1	5.6; 1.0	52
L^1									4.1; 2.1	58
L_3		51	46	-	49	59	libr			
L_{4-1}	46	51	52	49	49	52	trans	12.7; 3.1	6.9; 0.7	73
L_{4-2}	51							11.7; 3.4	3.0	81
L_5	60	59	59	60	59	55	trans	11.2; 2.2	3.3	93
L_{6-1}	69							12.3; 1.7	3.7	97
L_{6-2}	72	70	70	74	70	64	trans	14.0; 1.2	3.0	111
L_{6-3}	76							16.3; 6.8	6.1; 3.3	124
L^2									7.2; 1.6	118
L^3									6.0; 3.5	131

[a] Reference 23. [b] The values of the pressure coefficients are obtained from the polynomial or linear equation. Two values in the column correspond to the coefficients, respectively, at the beginning and the end of a particular pressure range.

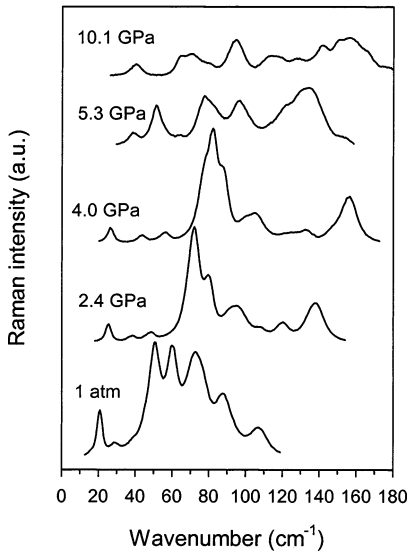

Figure 9. Raman spectra of external modes at several pressures. According to ref 23, two higher frequency peaks are internal modes, ν_{53} and ν_{54}. Pressure values (GPa) are shown next to each spectrum. The curves in this figure are vertically displaced for the sake of clarity.

across the sample, one can estimate the gradient across the sample to be as large as ~4.5 GPa at 22 GPa. Note that the highest frequency of the mode is found close to the center of the hole in the gasket.

Although the changes in the mode frequency are gradual across the sample, the changes in the mode width are quite inhomogeneous. The areas with different width of the Raman mode are randomly distributed over the sample. Seemingly, the changes in the width reveal the local changes in the crystal due to structural defects and/or chemical changes. On the other hand, the changes in the peak frequency correspond mainly to the pressure gradient on the sample. Upon the release of pressure to 1 atm, the spectrum fully recovered its shape and almost 90% of the initial intensity. Therefore, we conclude that non-hydrostatic compression to 22 GPa did not introduce any obvious irreversible structural and chemical changes to the RDX crystal.

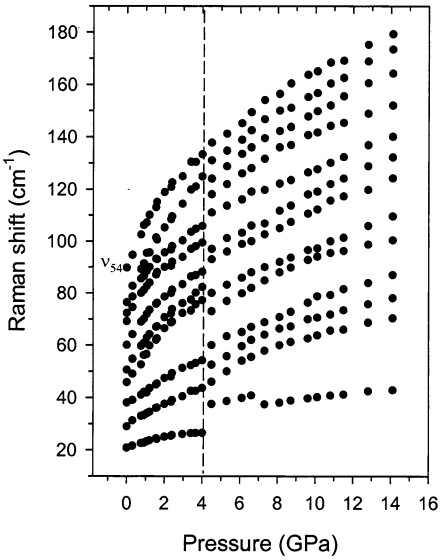

Figure 10. The effect of pressure on Raman shifts of external modes and the lowest frequency internal mode, ν_{54}. The vertical dashed line marks the onset of discontinuity.

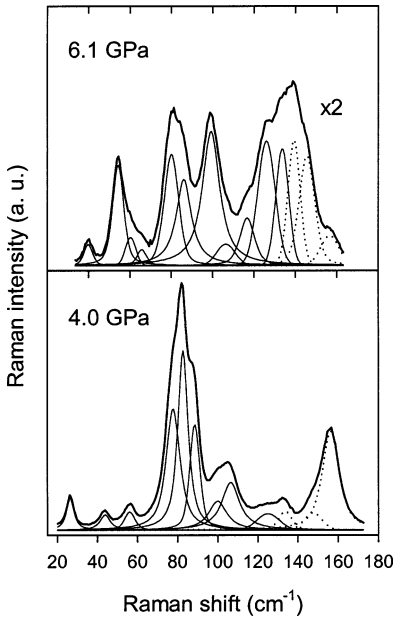

Figure 11. Example of separation of vibrational modes from the low-frequency spectra in α-phase (4 GPa) and γ-phase (6.1 GPa). The spectrum at 6.1 GPa was magnified by a factor of 2. Internal modes are denoted by dotted lines.

E. Discussion of Pressure Effect on Symmetry and Structure of RDX Crystal. Before we discuss possible implications of high pressure on the symmetry and structure of RDX, we briefly summarize the important results. The Raman data clearly display two distinct regions of pressure dependencies below and above 4 GPa. Below 4 GPa, the most sensitive internal vibrations with respect to pressure, on the basis of the pressure dependence of Raman shifts, are in order of decreasing frequency: CH-stretching, N−N-stretching, N−C-stretching, all ring, and NO_2-torsions. The NO_2-stretching vibrations are the least sensitive to changes of pressure. It is worth pointing out that both the CH- and NO_2-stretching vibrations of bonds in

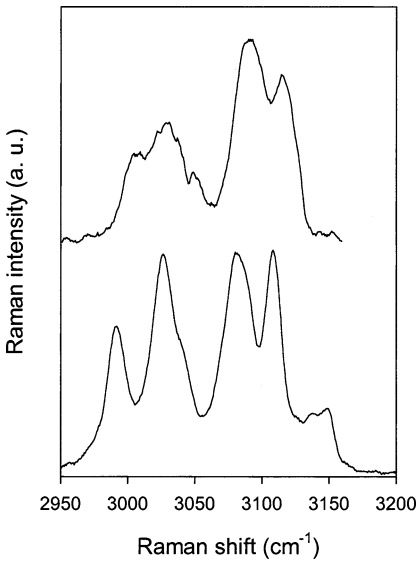

Figure 12. Raman spectra in the range of CH-stretching modes. Lower trace: spectrum under hydrostatic compression to 13.1 GPa. Upper trace: spectrum under non-hydrostatic compression to 13.2 GPa.

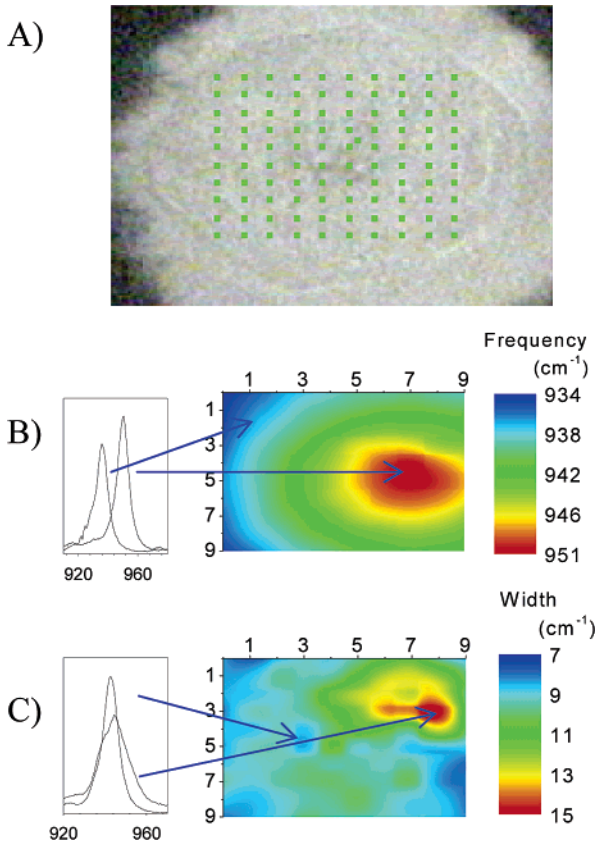

Figure 13. Spatial mapping of the C−N-stretching mode, ν_{32}, under non-hydrostatic compression to 22 GPa. (A) Image of the crystal in the gasket. The mapping area is 100 × 65 μm^2. Green spots indicate the position of the incident laser beam. (B) Spatial mapping of the mode frequency. (C) Spatial mapping of the mode width. On the left are the spectra taken at the indicated spots.

axial position are somewhat more affected by pressure than those in equatorial position (Table 1). At 4 GPa and above, several changes occur: (i) twofold splitting of many internal modes, both of A′ and A″ symmetry, (ii) no significant change in the number of external modes, and (iii) a large increase in sensitivity to pressure for the NO_2-stretching vibrations.

It is somewhat surprising that the NO_2-stretching vibrations, which are associated with the terminal atoms of the molecule and therefore more directly exposed to the reduction in intermolecular distances, are hardly influenced by an increase of pressure in the α-phase. This would suggest that either the NO bonds are already strained at ambient conditions or that the change in intermolecular interactions is weak. The data do not permit us to clarify this subject. However, it is noteworthy that NO_2-stretching vibrations for NO_2 groups in axial positions are somewhat more susceptible to a pressure increase than the vibrations for the NO_2 group in the equatorial position. Examination of the crystal structure of RDX at ambient conditions indicates that NO_2 groups in the axial position are in closer contact with atoms of the adjacent molecule (∼0.3 nm) than NO_2 groups in the equatorial position (∼ 0.32 nm).[2,34] Conceivably, this can contribute to the observed difference in sensitivity to pressure of stretching vibrations of NO_2 groups in axial and equatorial positions. In contrast to NO_2-stretching behavior, the NO_2-torsion vibrations exhibit one of the strongest dependences on pressure. Up to 4 GPa, the pressure dependence of Raman shifts decreases considerably, in close correspondence to changes in external modes (see remarks in Section IV). In summary, it appears that the main effect of pressure on the RDX structure below 4 GPa is a strong modification of NO_2 group torsion and gradual modification of bonding in the s-triazine ring together with the associated N−N bonds.

High pressure can destabilize the ambient RDX structure by disturbing the balance of the intermolecular interactions and the intramolecular distortions. Seemingly, at ∼4 GPa, the intramolecular strains no longer support the increase of repulsive contribution to the total energy. Thus, the phase transition is expected to relieve the repulsive interactions. A significant increase in the pressure dependence of NO_2-stretching vibrations may indicate that NO_2 groups underwent rearrangement leading to release of strain accumulated in the α-phase. This could be accomplished by the rotation/twist of the NO_2 groups on the molecules and/or the rotation/twist of the molecules themselves. Because almost every internal and external mode was affected by the phase transition (refer to Tables 1 and 2), it seems that the α−γ transition involves structural modification of both the molecules and their arrangement.

Another piece of information regarding the possible nature of changes in the RDX structure can be derived from mode splittings. The increase in the number of peaks (internal modes) in the Raman spectra is in general indicative of the lowering of molecular and/or crystal symmetry.[35] In the case of RDX, the peaks for many internal modes show twofold splitting in the γ-phase. In principle, two factors can contribute to the splitting of internal vibrations of molecules in the crystal. The first arises from the effect of site symmetry, which can result in lowering of the effective molecular symmetry and removal of degeneracies. The second arises from the effect of factor group coupling, which can result in the splitting of vibrations due to interactions between different molecules in the unit cell. The analysis of correlations between molecular, site, and unit cell symmetries can be useful in providing information about the crystal structure. However, it does not permit a unique choice of the space group.

To narrow down the possible unit cell symmetries of the γ-phase of RDX, we use the following practical assumptions: (i) molecular symmetry is not higher than in the α-phase, i.e., C_s or C_1, (ii) site symmetry is not higher than the molecular symmetry, and (iii) crystal structure is not higher symmetry than in the α-phase. The following structures are consistent with these assumptions:[36]

orthorhombic - $D_{2h}[C_1(8)]$, $D_{2h}[C_s(4)]$, $C_{2v}[C_1(4)]$, $C_{2v}[C_s(2)]$, $D_2[C_1(4)]$,

monoclinic - $C_{2h}[C_1(4)]$, $C_{2h}[C_s(2)]$, $C_s[C_1(2)]$, $C_s[C_s(1)]$, $C_2[C_1(2)]$,

triclinic - $C_i[C_1(2)]$, $C_1[C_1(1)]$.

In square brackets are given the site symmetries, along with the number of molecules on the site. The number of molecules in the unit cell determines the number of external modes in the crystal. Thus, one can find that each structure with one or two molecules per unit cell yields less than 12 Raman active external modes. For other structures, the number of predicted Raman external modes would be at least 12; i.e., 12 for $\{D_{2h}[C_s(4)], C_{2h}[C_1(4)]\}$, 21 for $\{C_{2v}[C_1(4)], D_2[C_1(4)]\}$, and 24 for $D_{2h}[C_1(8)]$. Because 12 Raman modes are observed in the γ-phase, in principle, five of these structures should all be considered as a potential high-pressure structure of RDX. However, based on the fact that the observed number of external modes in the α-phase differs significantly from the predicted number of modes in this phase (9 instead of 24), it is also unlikely that all predicted external modes are detected in the γ-phase. In other words, one would anticipate that the observed number of external modes in the γ-phase represents only a fraction of the predicted number of external modes. Therefore, it is reasonable to assume that the γ-polymorph has one of the structure from $D_{2h}[C_1(8)]$, $C_{2v}[C_1(4)]$, and $D_2[C_1(4)]$ with 24 or 21 external modes rather than the $D_{2h}[C_s(4)]$ or $C_{2h}[C_1(4)]$ structure with 12 external modes.

If the RDX molecules occupy general positions, i.e., C_1 site symmetry (as in the above three structures), then all selection rules and degeneracies for the molecule under its intrinsic symmetry are lost. Therefore, only factor group coupling can be responsible for the observed splitting of the internal vibrational modes. Examination of the correlation tables for the $D_{2h}[C_1(8)]$, $C_{2v}[C_1(4)]$, and $D_2[C_1(4)]$ factor groups indicates that these groups would cause fourfold splitting of each internal Raman active mode. Actually, twofold splittings are observed in the experiments, likely indicating that the magnitude of splitting is too small to permit resolution of all four peaks or that two other components may have very low intensity.

It is expected that the Raman and infrared (IR) vibrations should be coincidental for $C_{2v}[C_1(4)]$ and $D_2[C_1(4)]$ factor groups and non-coincidental for the $D_{2h}[C_1(8)]$ group. Therefore, the comparison between Raman and IR modes in the γ-phase could be useful in discriminating between the three proposed factor groups. Unfortunately, the available IR spectral data at 9.8 GPa[16] do not have adequate resolution to make an effective comparison with our Raman data. However, the available X-ray data demonstrate that the dimensions of the unit cell hardly change at the $\alpha-\gamma$ phase transition.[3] It would indicate that the number of molecules in the γ-phase remains the same as in the α-phase. The $C_{2v}[C_1(4)]$ and $D_2[C_1(4)]$ factor groups would require reduction of molecules in the unit cell from eight in α-phase to four in the γ-phase. Consequently, the only structure that preserves eight molecules in the unit cell is $D_{2h}[C_1(8)]$.

Although our data are not conclusive, we tend to favor a structure for the γ-phase of RDX that is orthorhombic with the space group isomorphous with the $D_{2h}[C_1(8)]$ point group rather than with the $C_{2v}[C_1(4)]$ and $D_2[C_1(4)]$ groups. Therefore, the factor group symmetry of the γ-polymorph seems to be the same as the α-polymorph. The changes in the γ-phase, probed by the Raman spectroscopy, indicate that factor group coupling may be responsible for the splitting of internal modes. The increased coupling relative to the α-phase may be caused by both intra- and intermolecular structural changes. These changes should, however, preserve the factor group of the low-pressure phase.

IV. Summary

Pressure effects on the Raman spectrum of RDX single crystals were examined, and changes in both the internal and external vibrations were determined up to 15 GPa under hydrostatic compression and up to 22 GPa under non-hydrostatic compression. It is proposed that the main effect of pressure on the RDX structure below 4 GPa is a strong modification of NO_2 group torsion and gradual modification of bonding in the s-triazine ring together with the associated N−N bonds. A number of abrupt changes in the spectra indicate strongly the onset of a phase transition at 4.0 ± 0.3 GPa. This value is in agreement with those obtained previously on RDX powder using X-ray[3,14] and vibrational spectroscopy.[6,8] Our results indicate that the space group of the γ-phase can be isomorphous with the $D_{2h}[C_1(8)]$, $C_{2v}[C_1(4)]$, or $D_2[C_1(4)]$ point group. On the basis of the available X-ray diffraction data and our data, the $D_{2h}[C_1(8)]$ structure is favored over the other structures; that is, the γ-polymorph may have an orthorhombic structure with eight molecules occupying the C_1 symmetry sites. Therefore, the point group symmetry of the γ-polymorph seems to be the same as for the α-polymorph. The changes in the γ-phase, probed by Raman spectroscopy, indicate that factor group coupling may be responsible for the observed splitting of internal modes. It seems that the $\alpha-\gamma$ transition involves structural modification of both the molecules and their arrangement. These modifications should, however, preserve the factor group of the low-pressure phase. Inevitably, X-ray diffraction measurements at high pressures are required to determine the exact structure of the γ-polymorph.

Acknowledgment. Dr. D. E. Hooks from Los Alamos is thanked for providing RDX crystals. We also thank Drs. J. M. Winey and J. E. Patterson for valuable discussion and comments. This work was supported by DOE Grant DEFG0397SF21388 and ONR Grant N000149310369.

References and Notes

(1) McCrone, W. C. *Anal. Chem.* **1950**, *22*, 954.
(2) Choi, C. S.; Prince, E. *Acta Crystallogr., Sect. B* **1972**, *28*, 2857.
(3) Olinger, B; Roof, B; Cady, H. In *Proceedings of International Symposium on High Dynamic Pressures*; Paris, France, 1978; p 3.
(4) Karpowicz, R. J.; Sergio, S. T.; Brill, T. B. *Ind. Eng. Chem. Prod. Res. Dev.* **1983**, *22*, 363.
(5) Karpowicz, R. J.; Brill, T. B. *J. Phys. Chem.* **1984**, *88*, 348.
(6) Baer, B. J.; Oxley, J.; Nicol, M. *High Pressure Research* **1990**, *2*, 99.
(7) Torres, P.; Mercado, L.; Cotte, I.; Hernandez, S. P.; Mina, N.; Santana, A.; Chamberlain, R. T.; Lareau, R.; Castro, M. E. *J. Phys. Chem. B* **2004**, *108*, 8799.
(8) Miller, P. J.; Block, S.; Piermarini, G. J. *Combust. Flame* **1991**, *83*, 174.
(9) Filhol, A.; Clement, C.; Forel, M.; Paviot, J.; Rey-Lafon, M.; Richoux, G.; Trinquecoste, C.; Cherville, J. *J. Phys. Chem.* **1971**, *75*, 2056.
(10) Shishkov, I. F.; Vilkov, L. V.; Kolonits, M;, Rozsondai, B. *Struct. Chem.* **1991**, *2*, 57.
(11) Rice, M. B.; Chabalowski, C. F. *J. Phys. Chem. A* **1997**, *101*, 8720.
(12) Harris, N. J.; Lammertsma, K. *J. Am. Chem. Soc.* **1997**, *119*, 6583.
(13) Vladimiroff, T.; Rice, B. M. *J. Phys. Chem. A* **2002**, *106*, 10437.
(14) Yoo, C. S.; Cynn, H.; Howard, W. M.; Holmes, N. In *Proceedings of the 11th International Detonation Symposium*; Snowmass, CO, 1998; p 951.
(15) Goto, N.; Yamawaki, H.; Tonokura, K.; Wakabayashi, K.; Yoshida, M.; Koshi, M. *Mater. Sci. Forum* **2004**, *465*, 189.
(16) Goto, N.; Yamawaki, H.; Wakabayashi, K.; Nakayama, Y.; Yoshida, M.; Koshi, M. *Sci. Technol. Energ. Mater.* **2005**, *66*, 291.
(17) Xu, J.; Mao, H. K. *Science* **2000**, *290*, 783.

(18) Barnett, J. D.; Block, S.; Piermarini, G. J. *Rev. Sci. Instrum.* **1973**, *44*, 1.
(19) Dreger, Z. A.; Trotman, N.; Gupta, Y. M. In preparation.
(20) Gupta, Y. M.; Shen, X. A. *Appl. Phys. Lett.* **1991**, *58*, 583.
(21) Park, T. R.; Dreger, Z. A.; Gupta, Y. M. *J. Phys. Chem. B* **2004**, *108*, 3174.
(22) Rey-Lafon, M.; Trinquecoste, C.; Cavagnat, R.; Forel, M. T. *J. Chim. Phys. Phys.-Chim. Biol.* **1971**, *68*, 1533.
(23) Rey-Lafon, M.; Cavagnat, R.; Trinquecoste, C.; Forel, M. T. *J. Chim. Phys. Phys.-Chim. Biol.* **1971**, *68*, 1575.
(24) Haycraft, J. J.; Stevens, L. L.; Eckhardt, C. J. *J. Appl. Phys.* **2006**, *100*, 053508.
(25) Patterson, J. E.; Dreger, Z. A.; Gupta, Y. M. To be submitted.
(26) *Molecular Systems under High Pressure*; Pucci, R., Piccitto, G., Eds.; North Holland, Amsterdam, 1991.
(27) Zallen, R. *Phys. Rev. B* **1974**, *9*, 4485.
(28) Zallen, R.; Slade, M. L. *Phys. Rev. B* **1978**, *18*, 5775.
(29) Hedoux, A.; Guinet, Y.; Capet, F.; Affouard, F.; Descamps, M. *J. Phys.: Condens. Matter* **2002**, *14*, 8725.
(30) Park, T. R.; Dreger, Z. A.; Gupta, Y. M. *J. Phys. Chem. B.* **2004**, *108*, 3174.
(31) Dreger, Z. A.; Lucas, H.; Gupta, Y. M. *J. Phys. Chem. B.* **2003**, *107*, 9268.
(32) Dreger, Z. A.; Balasubramaniam, E; Gupta, Y. M.; Joly, A. G. In preparation.
(33) Yoo, C. S.; Cynn, H. *J. Chem. Phys.* **1999**, *111*, 10229.
(34) Karpowicz, R. J.; Brill, T. B. *J. Phys. Chem.* **1983**, *87*, 2109.
(35) Decius, J. C.; Hexter, R. M. *Molecular Vibrations in Crystals*; McGraw-Hill Inc.: New York, 1977.
(36) Fateley, W.G.; Dillish, F.R.; McDevitt, N.T.; Bentley, F.F. *Infrared and Raman Selection Rules for Molecular and Lattice Vibrations: The Correlation Method*; J. Wiley & Sons: New York, 1972.